Pergamon

Cement and Concrete Research 32 (2002) 719–730

CEMENT AND CONCRETE RESEARCH

XRD, EDX and IR analysis of solid solutions between thaumasite and ettringite

S.J. Barnett[a], D.E. Macphee[a,*], E.E. Lachowski[a], N.J. Crammond[b]

[a]*Department of Chemistry, University of Aberdeen, Meston Walk, Aberdeen AB24 3UE, UK*
[b]*Building Research Establishment Limited, Garston, Watford WD2 7JR, UK*

Received 29 November 2000; accepted 26 November 2001

Abstract

Solid solutions between thaumasite and ettringite were prepared by methods analogous to those well established for the preparation of thaumasite and ettringite. The extent of immiscibility in this system is investigated by varying the Al:Si and SO_4^{2-}:CO_3^{2-} ratios in reactant mixtures. The solids produced were analysed by quantitative X-ray diffraction, with Rietveld refinement also providing accurate unit cell dimensions, energy-dispersive X-ray analysis and infrared spectroscopy. The compositional and unit cell variations in the solid solution are discussed. A wide variety of solid solution compositions were produced with both the thaumasite and ettringite structures, but all preparations were considerably diluted by secondary amorphous products.

Keywords: X-ray diffraction; EDX; Infrared spectroscopy; Thaumasite; Ettringite

1. Introduction

Thaumasite ($C_3S\bar{S}\bar{C}H_{15}$) and ettringite ($C_6A\bar{S}_3H_{32}$) are formed by the action of sulfates on cement and concrete [1–6]. In conventional sulfate attack [1], the monosulfate ($C_4A\bar{S}H_{12}$) in the cement reacts with external sulfate solutions to form ettringite, resulting in expansion and cracking. In the thaumasite form of sulfate attack (TSA) [2–6], calcium silicate hydrate, the main binding phase in the cement, reacts with aqueous carbonate and sulfate ions to form thaumasite. Consequently, TSA has also been observed in concrete made with sulfate-resisting Portland cement [2]. The attack results in softening and disintegration of the cement matrix.

Solid solutions between thaumasite and ettringite have been observed in several cases of TSA [2,4]. Thaumasite–ettringite solid solutions have also been found in nature [7] and have been produced in laboratory studies [8–10]. The range of solid solutions possible in this system is presently unknown. A miscibility gap is thought to exist because the thaumasite and ettringite structures, though very similar, have different symmetries [10–12]. The similarity of the X-ray diffraction (XRD) patterns and the formation of solid solutions make it likely that TSA has been misdiagnosed as conventional sulfate attack in the past.

The structures of thaumasite and ettringite were determined by Edge and Taylor [11] and Moore and Taylor [12], respectively. Both structures have been refined more recently [13–15], with the reported structures agreeing with the earlier works except in the fine structural detail. Thaumasite has a crystal structure based on columns of composition $[Ca_3Si(OH)_6{\cdot}12H_2O]^{4+}$ with the SO_4^{2-} and CO_3^{2-} anions lying in an ordered arrangement in channels between the columns. It is hexagonal with $a = 11.054$ Å and $c = 10.410$ Å [11,13,16]. The thaumasite structure is of interest crystallographically since it contains Si octahedrally coordinated by O. The ettringite structure is similar with Al replacing Si in the columns and $3SO_4^{2-}$ plus $2H_2O$ replacing $2SO_4^{2-}$ plus $2CO_3^{2-}$ in the channels. It is trigonal with $a = 11.234$ Å and $c = 21.501$ Å [12,16]. A detailed comparison of the thaumasite and ettringite structures in relation to solid solution formation was described by Barnett et al. [10]. Solid solution between thaumasite and ettringite involves replacement of silicon by aluminium and replacement of sulfate/carbonate by sulfate/water. It is possible that the replacements of Si and SO_4^{2-}/CO_3^{2-} are partly or completely independent of each other, i.e., that the sulfate:carbonate ratio is independent of

* Corresponding author. Tel.: +44-1224-272-941; fax: +44-1224-272-921.
E-mail address: d.e.macphee@abdn.ac.uk (D.E. Macphee).

0008-8846/02/$ – see front matter
PII: S0008-8846(01)00750-5

the silicon:aluminium ratio, while the total SO_4^{2-} plus CO_3^{2-} changes to maintain charge balance. This will be discussed in a later paper [17].

The work presented here aims to determine the possible range of compositions of solid solutions between thaumasite and ettringite. Solid solutions have been prepared by methods analogous to those reported in the literature [16] for the production of thaumasite and ettringite, with both the Si:Al and SO_4^{2-}:CO_3^{2-} ratios in the starting mixes being varied incrementally between the two end members. Techniques sensitive to solid solution effects in mixtures of phases were used to analyse the solids produced, namely XRD and transmission electron microscopy. Infrared (IR) spectroscopy has also been applied to these solids. The presence of absorption bands due to octahedral silicon in the IR spectrum provides a means of quantifying the miscibility gap in the solid solution, since all the octahedral Si present are in the thaumasite/ettringite and will not be present in any contaminating material.

2. Preparation of materials

The preparation of solid solutions between thaumasite and ettringite was carried out at 5 °C by methods analogous to those published [16] for synthesising the end members.

Eleven mixes, ranging from ettringite to thaumasite, were prepared according to Table 1 to provide a range of Si:Al ratios. For each mix, a slurry of 6.70 g of calcium oxide (obtained by firing Analar $CaCO_3$) in 445 cm^3 10% wt/wt sucrose solution was mixed with a slurry containing the required amounts of sodium silicate (reagent grade $Na_2Si_2O_5{\cdot}2H_2O$), sodium aluminate (reagent grade $NaAlO_2$), sodium sulfate (Analar Na_2SO_4) and sodium carbonate (Analar Na_2CO_3) in 20 cm^3 water. The amounts of silicate, aluminate, sulfate and carbonate were varied incrementally between the end members of the solid solutions, as described in Table 1. Ettringite itself was prepared slightly differently, by mixing the calcium oxide slurry with one containing 12.57 g of aluminium sulfate hydrate (Analar $Al_2(SO_4)_3{\cdot}16H_2O$).

In order to exclude atmospheric carbon dioxide, all preparations were carried out under a nitrogen blanket. The calcium oxide used was freshly prepared by firing Analar $CaCO_3$ at 1000 °C overnight and the water used was boiled, double-distilled and allowed to cool under nitrogen before use.

The mixes were sealed in high-density polyethylene bottles. The ettringite-based end member formed almost immediately after mixing. All the other mixes were stored at 5 °C for 6 months with periodic agitation. Samples of the solids produced were isolated by suction filtration, carried out under nitrogen. The solids were then washed with distilled water and dried over silica gel in a desiccator at room temperature.

3. XRD and Rietveld refinement

Samples of the solids were prepared for QXRD analysis by being lightly ground with corundum (α-Al_2O_3) and side-loaded into a sample holder (to minimise preferred orientation). XRD patterns were collected using Cu Kα radiation with a Philips PW1730 diffractometer over the angular range 4–60° 2θ, with a step size of 0.04° 2θ and a count time of 4 s per step. Rietveld refinement was carried out using the commercially available SIROQUANT software package [18]. The single crystal structure determinations for thaumasite and ettringite, carried out by Edge and Taylor [11] and Moore and Taylor [12], respectively, were used as starting models in the refinement procedure. The refinement procedure provides quantitative phase analysis and accurate unit cell dimensions for the solid solution phases [19].

Fig. 1 shows small sections of the XRD patterns of a number of solids. The figure highlights the changes that take place in the XRD patterns as a result of solid solution effects. In some of the solids produced, two distinctive solid solution structure types were present, while in solids close to the end member preparations, one solid solution phase was formed. These are subsequently referred to as ‘thaumasite-type’ and ‘ettringite-type’ phases. The changing quantities of these two phases are clear from their relative intensities in Fig. 1. The

Table 1
Composition of starting mixes

Series	Si:Al molar ratio	SO_4^{2-}:CO_3^{2-} molar ratio	Mass of $Na_2Si_2O_5{\cdot}2H_2O$ (g)	Mass of $NaAlO_2$ (g)	Mass of Na_2SO_4 (g)	Mass of Na_2CO_3 (g)
1	100:0	50:50	4.34	0.00	5.65	4.23
	90:10	54:46	3.91	0.33	5.93	3.81
	80:20	58:42	3.47	0.65	6.22	3.38
	70:30	62:38	3.04	0.98	6.50	2.96
	60:40	67:33	2.60	1.31	6.78	2.54
	50:50	71:29	2.17	1.64	7.07	2.12
	40:60	76:24	1.74	1.96	7.35	1.69
	30:70	82:18	1.30	2.29	7.63	1.27
	20:80	88:12	0.87	2.62	7.91	0.85
	10:90	93:7	0.43	2.94	8.20	0.42

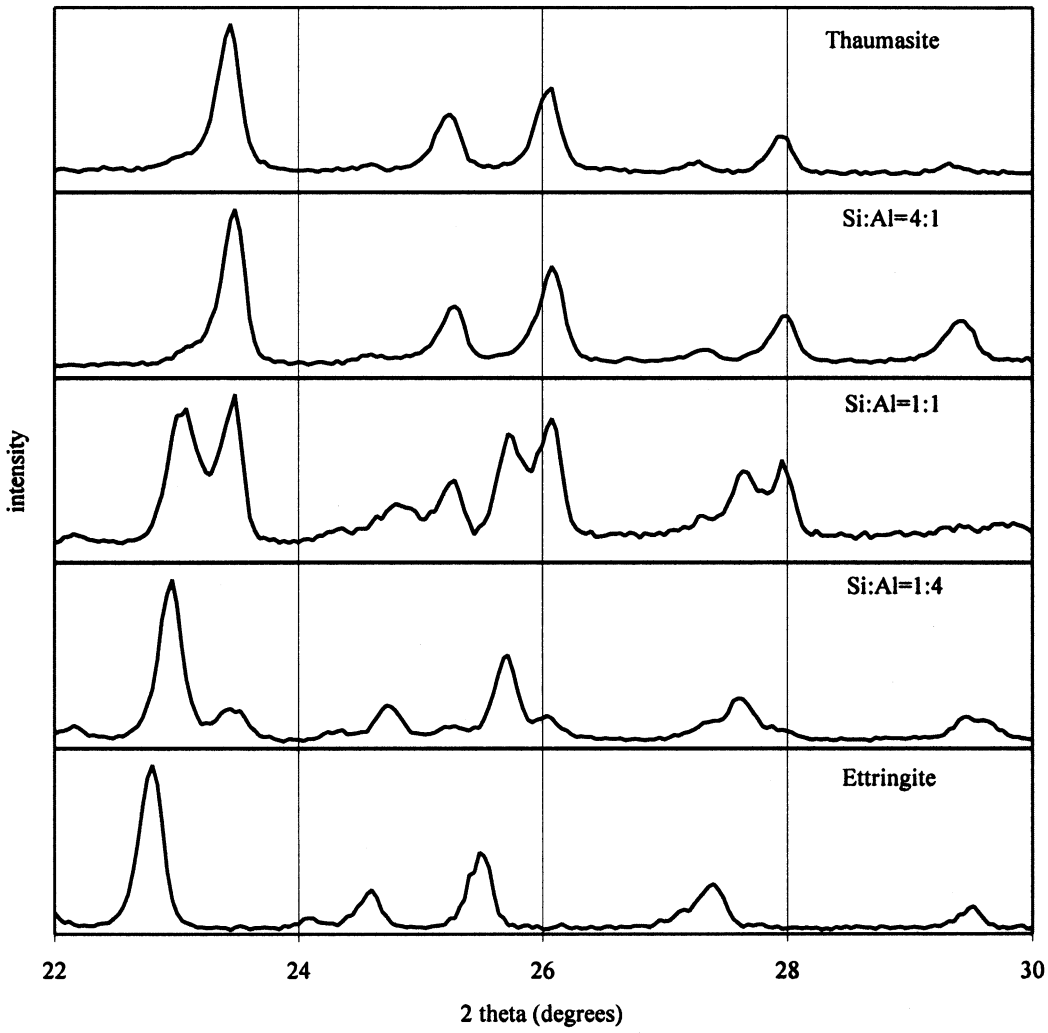

Fig. 1. Partial XRD patterns of solid solutions. Si:Al ratios refer to starting mixture compositions as defined in Table 1.

figure also emphasises the solid solution effects on structure, observed by XRD, since the positions of the peaks due to each phase are changing. This suggests that compositional variations are affecting the unit cell parameters of both phases.

In Rietveld refinement, the 'thaumasite-type' phase was assumed to have the thaumasite structure and the 'ettringite-type' phase the ettringite structure. Corundum was included in the refinement procedure, as well as calcite, which was present in some samples. The parameters refined were: zero point error, scale factors, unit cell parameters, peak width and shape parameters. Fig. 2 shows an example of the graphical output of the Rietveld procedure, illustrating the agreement between calculated and observed data. This figure is typical of the quality of fit obtained ($\chi^2 \sim 5\%$) in samples containing two distinct solid solution phases. No attempt has been made in this work to refine the atomic positions or occupancies of the thaumasite/ettringite structures. Therefore, any changes in relative intensities caused by changing composition have not been studied. Peak intensities would not necessarily change uniformly with composition in a complicated system such as this. Also the presence of two very similar phases makes accurate assignment of peak intensities impossible because of overlapping of reflections. While it may be possible to refine sulfate/carbonate ratios by this technique, the similarity in size of aluminium and silicon would make refinement of the Si:Al ratio by Rietveld methods meaningless. The XRD work therefore concentrates on the changes in unit cell dimensions caused by solid solution effects, which are more easily measured, and on quantitative phase analysis of the mixtures.

Weight ratios of the crystalline phases are automatically outputted by the Rietveld refinement procedure and were used to calculate the quantities of ettringite/thaumasite, any crystalline impurities and amorphous material (by difference) in the solid. Fig. 3 shows the quantitative XRD results, indicating the amounts of the solid solution phases present as well as impurity phases (calcite and amorphous material). All the solids were found to contain a considerable level of amorphous material, and the amount of amorphous material present increases sharply close to the

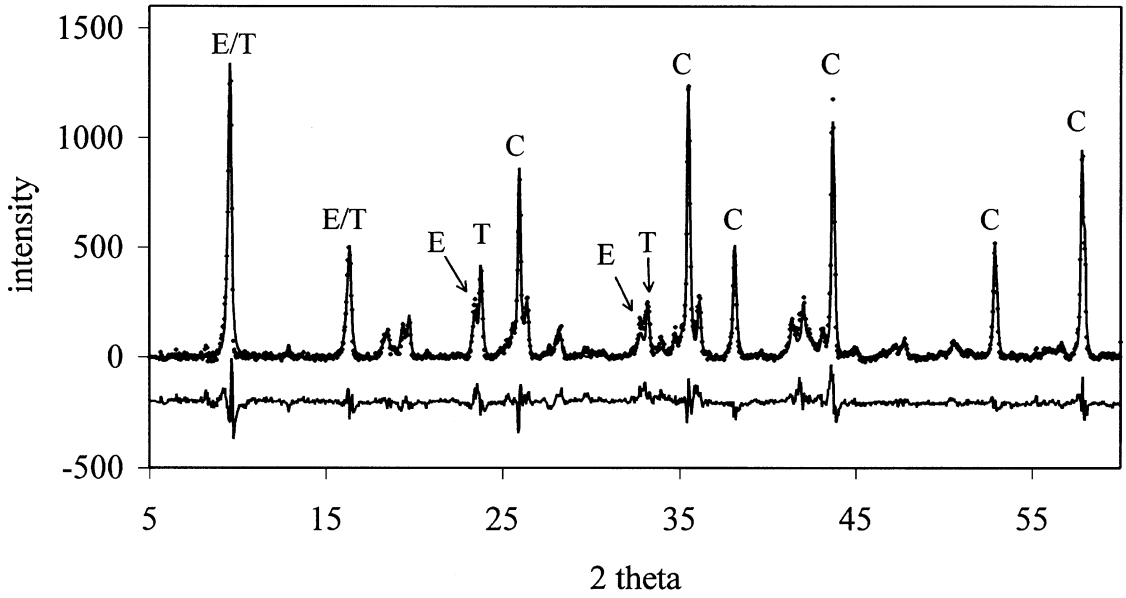

Fig. 2. Results from Rietveld refinement of solid solution prepared with Al:Si = 2:3 and SO_4^{2-}:CO_3^{2-} = 2:1. Legend: cross — observed; line — calculated; lower plot — difference. Main ettringite-like (E), thaumasite-like (T) and corundum (C) peaks are highlighted.

thaumasite end of the series. In these samples, $CaCO_3$ was also detected. The preparation of the thaumasite end member was found to contain only 25% by weight thaumasite.

Fig. 4 shows the refined unit cell parameters in graphical form. The graph shows the unit cell parameters of the solid solution phases plotted against each other (*c* versus *a*). To aid comparison, the *c*-dimensions of the thaumasite-like phases have been doubled.

The solid solution phases formed lie roughly on a line between the thaumasite and ettringite end members, with a large gap between two separate clusters. This gap corresponds to unit cell parameters $a = 11.08–11.14$ Å and $c = 20.9(10.45)–21.25$ Å. In the samples where two phases were formed, one phase lies in the 'thaumasite' cluster ($a < 11.08$ Å) and one lies in the 'ettringite' cluster ($a > 11.14$ Å). The gap between the two clusters is believed

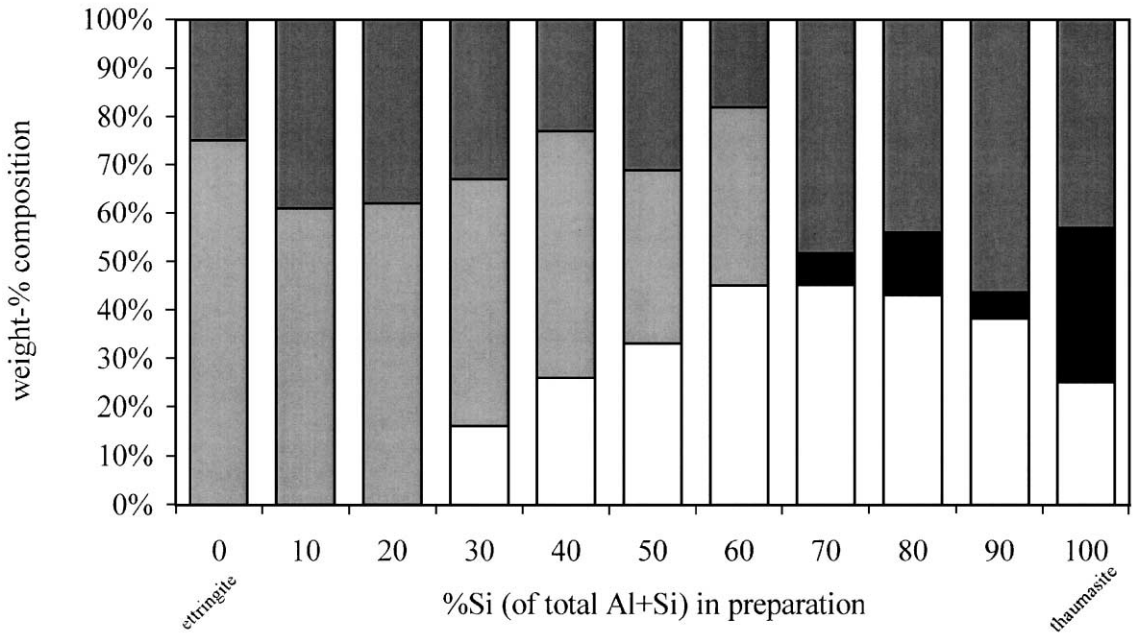

Fig. 3. Quantitative XRD corresponding to solids precipitated from starting solutions as defined in Table 1. Legend: white — thaumasite; light grey — ettringite; black — calcite; dark grey — amorphous.

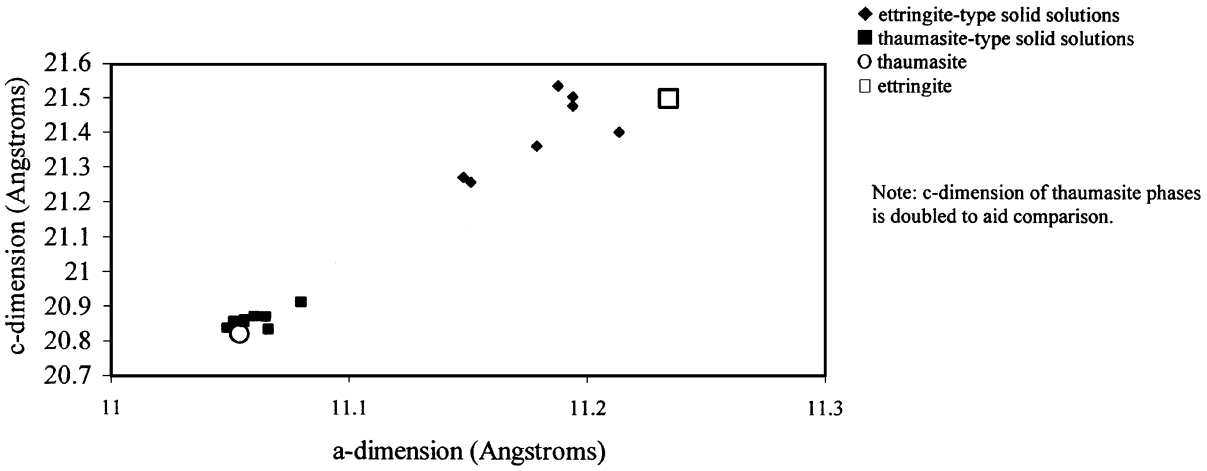

Fig. 4. Unit cell parameters of solid solutions. Legend: solid diamond — ettringite-type solid solutions; solid square — thaumasite-type solid solutions; hollow circle — thaumasite; hollow square — ettringite. *c*-dimension of thaumasite-type phases is doubled to aid comparison.

to correspond to the change in symmetry between ettringite and thaumasite.

4. Energy-dispersive X-ray (EDX) analysis

EDX analysis was carried out using a Link attachment on a JEOL 2000EX transmission electron microscope. Samples were prepared by dispersing a small amount of solid in isopropanol in a test tube and agitating for several minutes in an ultrasonic bath. A small amount of this suspension was then placed on a carbon-coated copper grid and allowed to dry. Analytical data were collected for 20–30 single, isolated crystals in each sample.

Electron microscopy identified crystals of two different morphologies in the solid solution samples, identified in Fig. 5:

- Type 1 — short, stubby crystals, considered to be 'ettringite';
- Type 2 — acicular crystals, considered to be 'thaumasite' [9].

The two morphologies were observed to co-exist in the samples identified as containing two different solid solution phases by XRD. Where only one phase was observed by XRD, only one morphology existed.

EDX analysis of Ca, Si, Al and S showed no clear dependence of the morphologies on composition. In some cases, the two morphologies clearly had different compositions, while in others they appeared to have the same composition. In general, the acicular crystals tended to have higher Si and lower SO_4^{2-} contents than the stubbier crystals.

The composition of the solids, as measured by EDX, is shown in Figs. 6 and 7. Fig. 6 shows the average S and Si contents of the solids. Fig. 6 suggests a systematic deficiency in SO_4^{2-} levels, which could be due to higher-than-expected substitution for CO_3^{2-} (or OH^-). Fig. 7 shows the Si and Al contents for all the individual crystals analysed. In Fig. 7, it can be seen that the short, stubby crystals (Type 1) are concentrated at higher Al contents, while the acicular crystals (Type 2) have higher Si levels.

Fig. 5. Transmission electron micrograph of a solid solution sample.

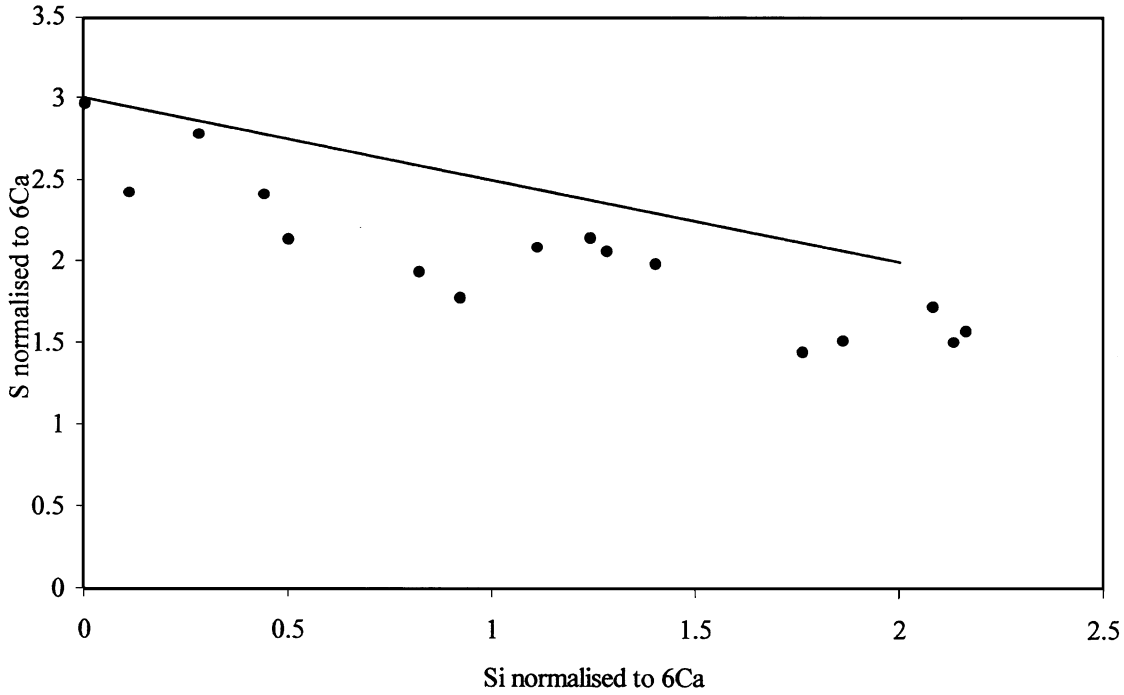

Fig. 6. Mean S versus Si for solid solutions. Legend: circle — measured; line — expected.

There is a considerable degree of overlap of the compositions of the two morphologies at intermediate Al/Si levels. No clear gap in the solid solution was observed.

In many cases, especially close to the thaumasite end of the solid solutions, the average Si content is higher than expected and the total (Al + Si) is greater than the theoretical value of 2. The excess Si observed could result from interference from secondary amorphous phases or from the presence of tetrahedral silicate anions in the channels of the structure [20]. In either case, any excess Si would be present in tetrahedral coordination with O, rather than the octahedral coordination in the solid solution phase of interest. It could therefore be detected by techniques sensitive to coordination environment, e.g., IR spectroscopy and NMR.

5. IR data collection and analysis

Fourier transform infrared (FTIR) spectroscopy was carried out using an ATI Mattson Genesis Series FTIR transmission instrument. Samples were prepared for analysis by grinding a known mass of solid with dried KBr. The resulting powder was then pressed at 2000 psi for 5 min to produce a pellet for analysis. IR data were collected by summing 16 scans over the wavenumber range 400–4000 cm^{-1}.

Some of the resulting IR spectra are illustrated in Fig. 8. Absorption bands were identified by reference to previously published IR data on ettringite and thaumasite [21–24], where possible, and by reference to other more general information [25,26]. Table 2 gives the wavenumbers of the important bands. Absorption bands due to tetrahedral Si were identified in samples close to the thaumasite end of the series — the same samples where excess Si was detected by EDX and a drop in crystallinity occurred. We may therefore conclude that the excess Si observed by EDX is contained within the amorphous phase in these solids.

For IR data analysis, the transmission spectra were transferred to a spreadsheet package (Microsoft Excel) and first converted to absorbance spectra. A procedure was devised to quantify the octahedral Si bands in the spectra, which involves the least squares fitting of the experimental data to a calculated spectrum produced by mixing experimental ettringite and thaumasite[1] spectra:

$$I_{ci} = X(I_{ei}) + Y(I_{ti})$$

where I_{ci} is the calculated absorbance at wavenumber i; I_{ei} and I_{ti} are the measured absorbances of ettringite and thaumasite, respectively, at wavenumber i; and X and Y are variables. The value $\sum(I_{ci} - I_{oi})^2$ was then minimised for the wavenumber range 475–525 cm^{-1} (corresponding to the 500 cm^{-1} SiO_6 band) by varying the values X and Y. Since only thaumasite (I_{ti}) contributes to the intensity of the SiO_6 absorption band in the calculated pattern, the value of Y is proportional to the amount of octahedral Si present and hence the 'thaumasite' content of the solid solution. Fig. 9 shows the level of agreement between calculated and observed spectra in the 400–1500 cm^{-1} region.

[1] The thaumasite spectrum used in the calculated pattern is a high-purity natural sample from Crestmore, CA.

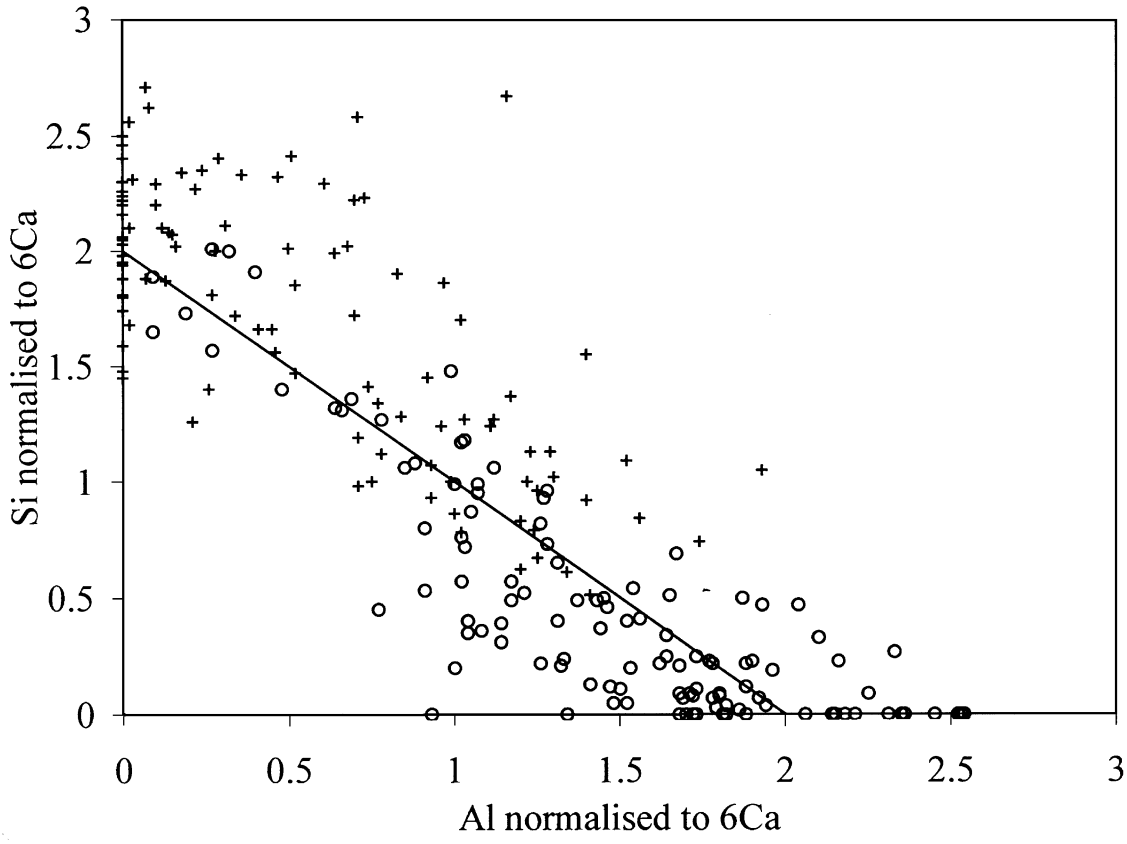

Fig. 7. Si versus Al for solid solutions; all analyses shown. Legend: circle — Type 1 morphology; cross — Type 2 morphology; line — expected.

A calculation was then performed to obtain the octahedral silicon content of the ettringite/thaumasite phase in the solid:

$$\text{moles octahedral Si in ettringite/thaumasite} = Y\frac{\text{moles}_{\text{std}} \times \text{mass}_{\text{std}}}{\text{mass}_{\text{e/t}}}$$

where $\text{moles}_{\text{std}}$ = moles octahedral Si in 2 mol of standard thaumasite = 2; mass_{std} = mass of standard; $\text{mass}_{\text{e/t}}$ = mass ettringite/thaumasite in sample (calculated from measured total mass of sample and QXRD crystallinity).

The results are presented in Fig. 10. The good agreement of the results close to the thaumasite end with the maximum possible octahedral silicon level shows that this method provides a valid route to the measurement of octahedral Si in the solid solution.

6. Miscibility gap

The results presented in Fig. 10 show the octahedral Si levels in the ettringite/thaumasite phases prepared. For the single-phase systems, these values directly provide the composition of the solid solution. However, for the two-phase systems, represented by the dotted region in Fig. 10, the values obtained give only an average octahedral Si level of the two phases. It is not possible to measure directly the degree of solid solution in each phase. However, it is assumed that the compositions of solids at the ends of the single-phase regions on either side of this gap lie close to the limits of the solid solution between thaumasite and ettringite, and that the two-phase systems are simply mixtures of these two compositions. In order to test this assumption, the octahedral silicon levels measured in the proposed limiting compositions were used, in conjunction with the relative amounts of ettringite- and thaumasite-type phases in the two-phase systems (measured by QXRD), to calculate n_{avg}, the expected average octahedral silicon:

$$n_{\text{avg}} = \frac{\%\text{ett}}{100} \times n_{\text{ett}} + \frac{\%\text{thaum}}{100} \times n_{\text{thaum}}$$

where %ett and %thaum are percentage ettringite-like and thaumasite-like character, respectively (from QXRD results), and n_{ett} and n_{thaum} are the number of moles of octahedral Si in the ettringite and thaumasite limits of the miscibility gap.

The results of this calculation are also shown in Fig. 10, alongside the measured values. The good agreement confirms the assumption that the single-phase limiting compositions on either side of this ‘gap’ are very close to the limits of the miscibility gap.

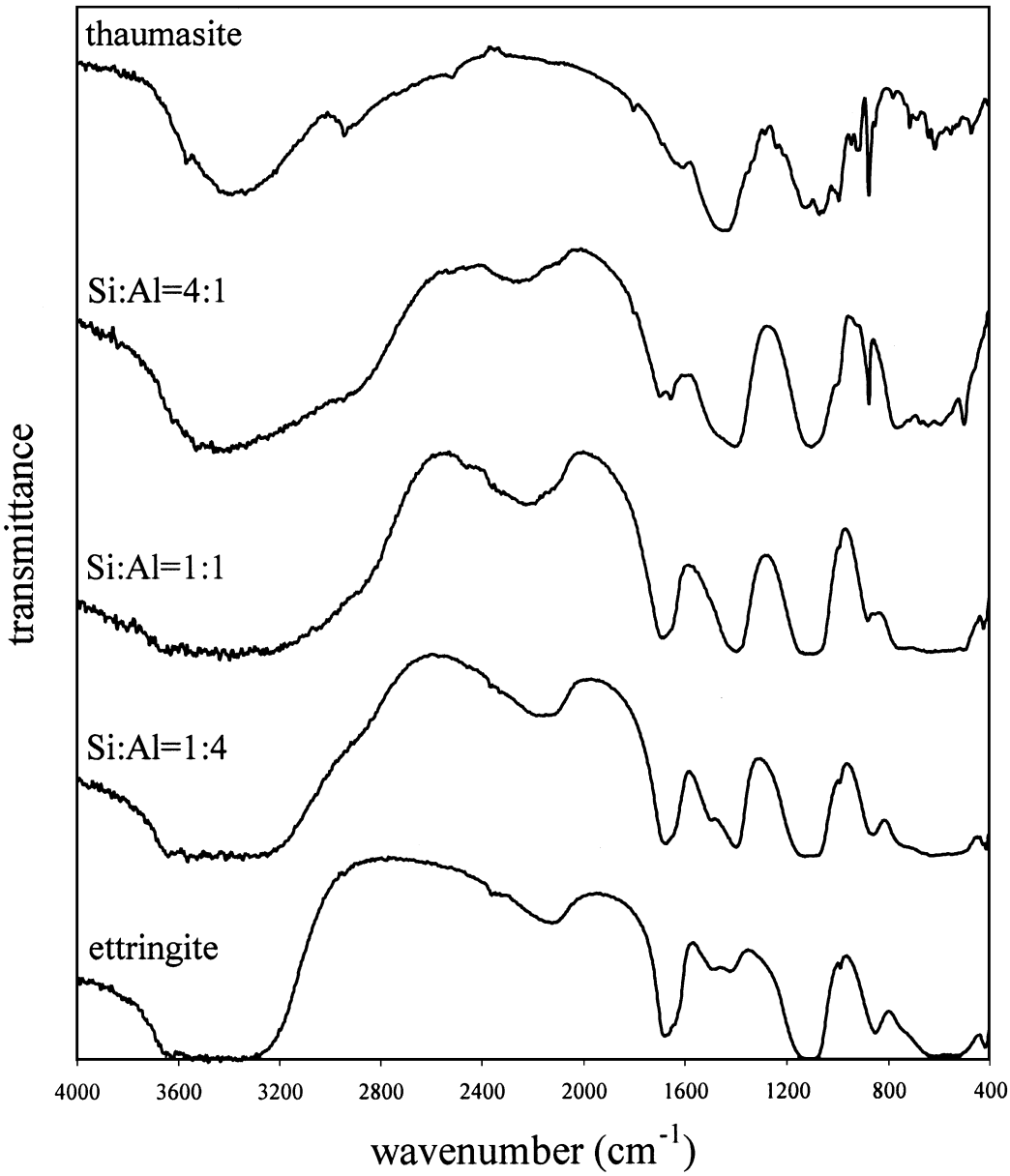

Fig. 8. IR spectra of thaumasite–ettringite solid solutions. Si:Al ratios refer to starting mixture compositions as defined in Table 1.

This evidence therefore defines a miscibility gap between Al:Si mole ratios of 1:1 and 1:7 (50% and 87% replacement of aluminium by silicon). The extent of the solid solution between thaumasite and ettringite is illustrated in Fig. 11, in which the miscibility gap is marked by a dotted line. The Si:Al ratios in the starting mixes are shown and highlight the difference between the expected and observed Si:Al ratios in the solid solutions. The thaumasite structure tolerates the replacement of 1/8 of its Si by Al, while the ettringite structure tolerates the replacement of 1/2 of its Al by Si.

Fig. 11 shows that, on the ettringite side of the miscibility gap, no ettringite was produced with replacement of between 6% and 50% of the aluminium by silicon. Three samples were prepared, which could be expected to fall in this region, but they all contained a higher octahedral silicon content than expected. Although we have not investigated

Table 2
Wavenumbers of important absorption bands

Wavenumber/cm^{-1}	Assignment
3600–3200	O–H stretch
1680	O–H bend
1400	C–O stretch (CO_3^{2-})
1100	S–O stretch (SO_4^{2-})
940/920	SiO_4
875	C–O bend (CO_3^{2-})
850	AlO_6
750	SiO_6 stretch
500	SiO_6 bend

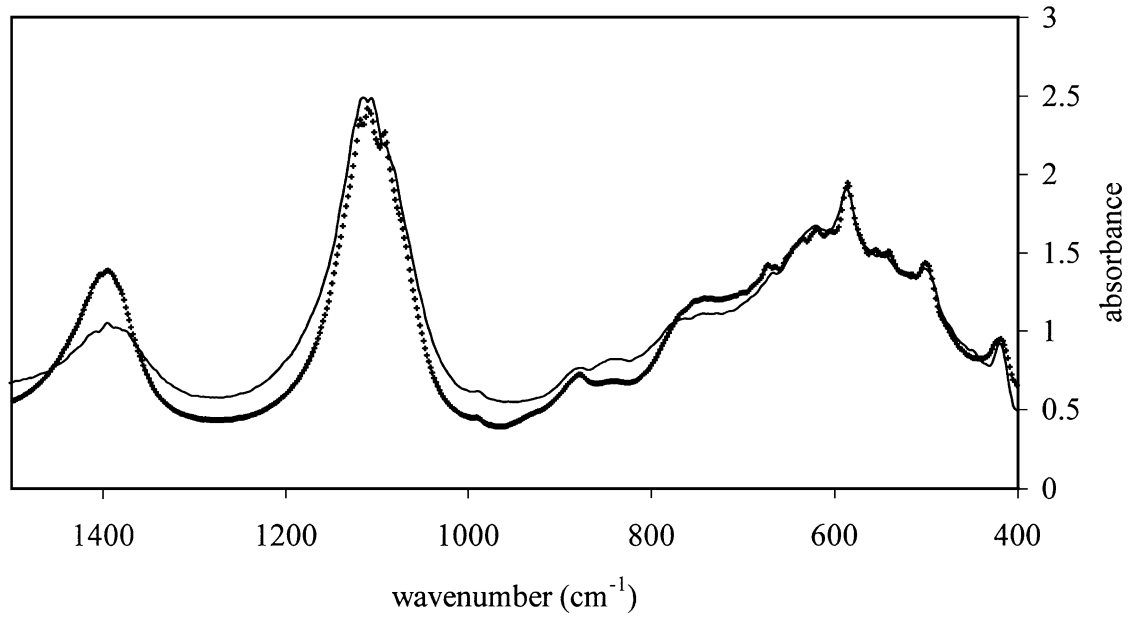

Fig. 9. Comparison of observed and calculated spectra for sample prepared with Si:Al = 1:4. Legend: cross — observed; solid line — calculated.

this specifically, this could be explained by the presence of the other phases, which may alter the equilibrium in such a way that the ettringite-type phase contains a higher-than-expected level of silicon. Alternatively, the ettringite-type phase is more stable with a higher level of Si than with a lower one. The ettringite structure has two crystallographically distinct aluminium sites [12]. The apparently favoured composition of a 1:1 Al:Si ratio could therefore be due to an ordered structure being preferred in which one of the two sites contains Al, while the other contains Si.

From a consideration of the crystal structures of thaumasite and ettringite [10–15], there is no reason why Si and Al cannot freely replace each other in the two structures, except that they have different charges. The difference in symmetries of thaumasite and ettringite is due to the different ordering of the anions in the channels of the structures. The total charge

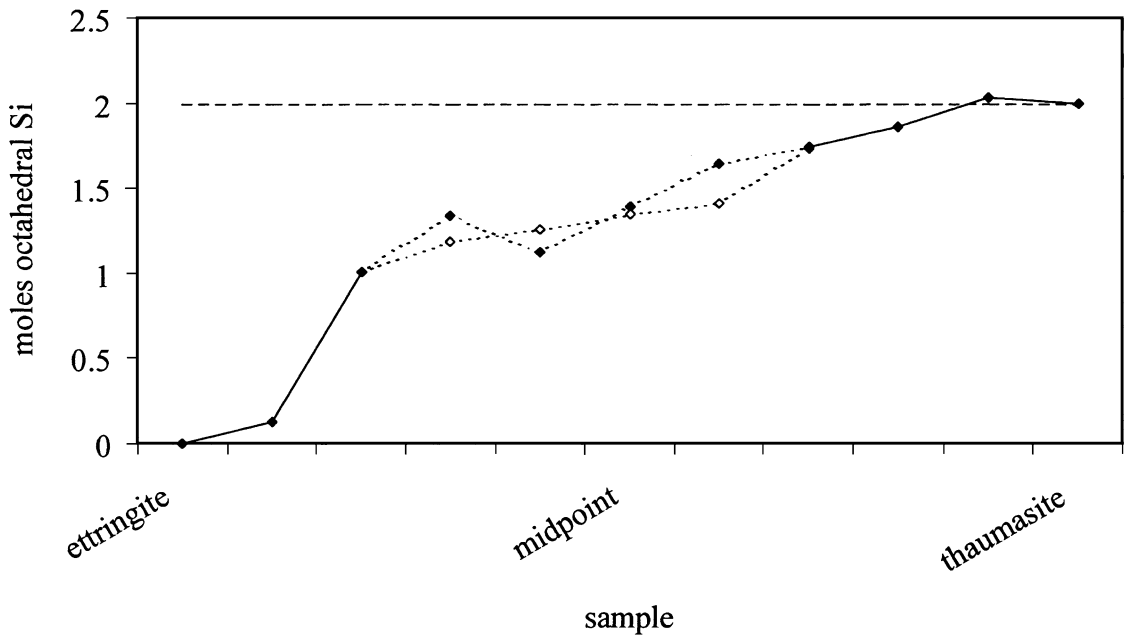

Fig. 10. Octahedral Si levels measured in thaumasite/ettringite phases. Legend: dashed line — maximum level; solid diamond — measured values; hollow diamond — calculated values; dotted line — two-phase region.

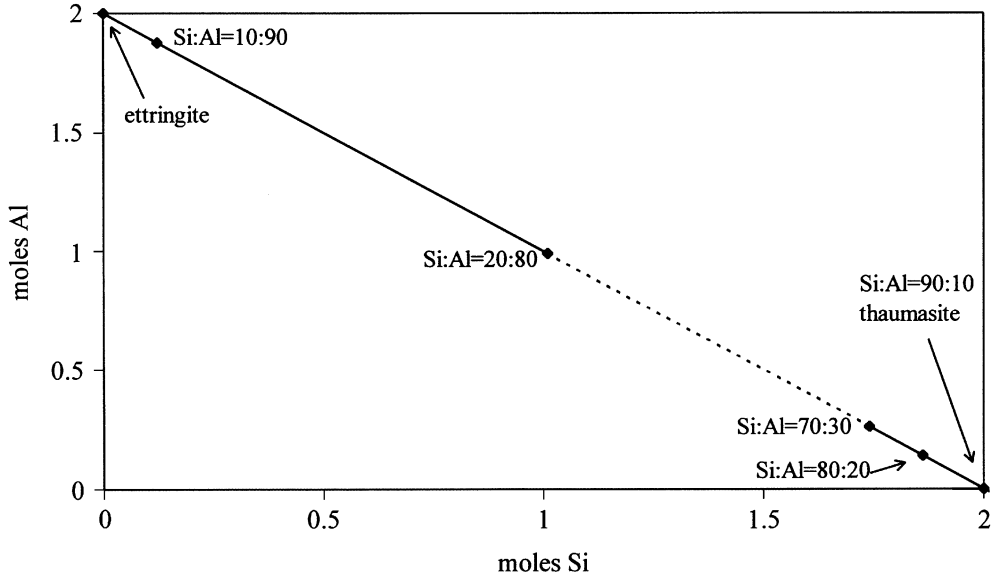

Fig. 11. Miscibility gap in the thaumasite–ettringite solid solution. Legend: Dotted line represents miscibility gap between thaumasite and ettringite. Si:Al ratios refer to starting mixture compositions as defined in Table 1.

(and hence the number) of anions in the channels has to change to balance the effects of varying the Al:Si ratio. In an ettringite-based solid solution, the levels of anions in the channels must increase when Al is replaced by Si. The excess anions presumably replace the two water molecules in the channels of the structure. In thaumasite-based solid solutions, a deficiency of anions would be needed to balance the replacement of Si by Al. [A Si:Al ratio of 7:1 (the maximum degree of solid solution in thaumasite observed in this work) would require an anion occupancy of 96.875%.] In either of these two scenarios, the structures could become unstable, leading to the observed miscibility gap. The effects of altering the anion SO_4^{2-}:CO_3^{2-} ratios in the starting mixes will be described in a later paper [17].

7. Comparison of techniques

The combination of QXRD and IR spectroscopy described above has provided a tool for the quantification of octahedral Si in the solid solution phases described in this work, which in turn identified a miscibility gap. Due to the

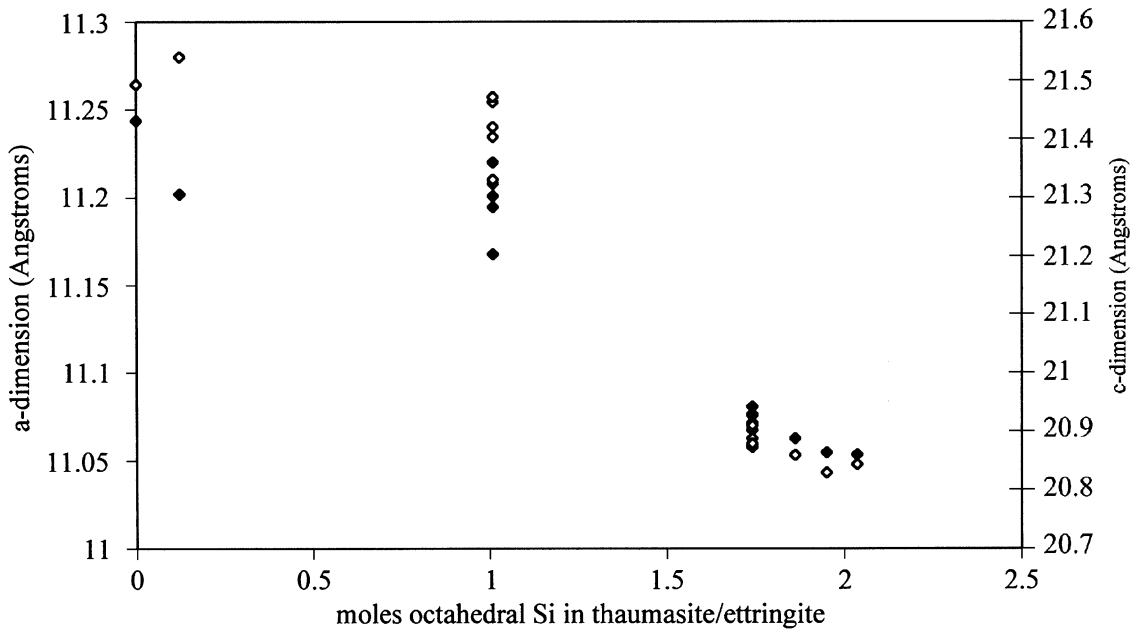

Fig. 12. Comparison of unit cell dimensions (XRD) and octahedral Si levels (IR). Legend: solid diamond — *a*-dimension; hollow diamond — *c*-dimension.

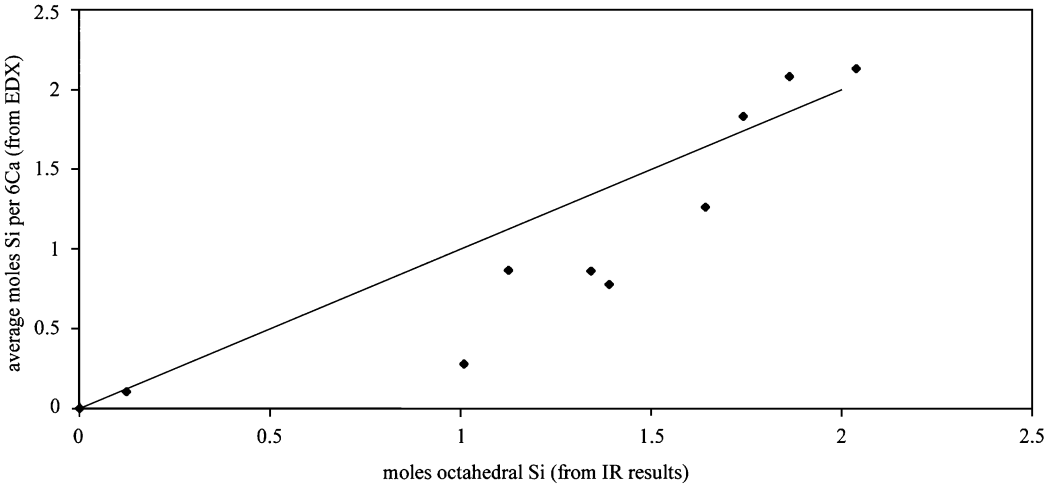

Fig. 13. Comparison of Si levels obtained by EDX and IR. Legend: diamond — actual values; line — ideal.

presence of large amounts of amorphous material, the IR technique alone cannot be used to determine the degree of solid solution in these systems. The QXRD data are required so that the amount of the solid solution phases in each solid can be determined.

Fig. 12 shows the relationship between unit cell parameters and the degree of solid solution determined by IR. The unit cell dimensions can be seen to vary with composition and are not constant at the limiting compositions of the solid solution. The variation in unit cell parameters cannot be directly related to Si content because the SO_4^{2-}:CO_3^{2-} ratio is also changing. The measurement of unit cell parameters provides little quantitative information on the degree of solid solution in relation to Al/Si content because the exchange of SO_4^{2-} for CO_3^{2-} (or possibly OH^-) is likely to have a much larger effect on the unit cell parameters. Also in structures such as these, the unit cell parameters do not change linearly with composition [27,28].

Comparison of the EDX and IR results (Fig. 13) shows the correct trend, although there is some deviation between the two data sets. It is noted, however, that the errors associated with the EDX technique are large and statistical analysis of the EDX data shows that the solids are inhomogeneous. The amorphous material present cannot be observed by TEM and no information is available on its composition. Therefore, it is possible that the amorphous phase is closely associated with the thaumasite/ettringite crystals and interferes with the analytical results obtained by EDX.

8. Conclusions

The XRD/Rietveld results confirm the presence of solid solutions between ettringite and thaumasite. Two structure types, having predominantly ettringite-like and thaumasite-like XRD patterns, were distinguished. The simultaneous occurrence of both in certain preparations suggests the presence of a miscibility gap in the solid solution.

The unit cell parameters of both the ettringite-like and thaumasite-like phases vary a great deal from the end members of the solid solution and a ‘gap’ exists in the variation of unit cell dimensions between the two structure types. This is believed to correspond to the change in symmetry between thaumasite and ettringite and to provide an explanation for immiscibility in this system.

In combination with XRD, FTIR has allowed us, for the first time, to identify the extent of immiscibility. Despite the preparations being impure, it was possible to show that the thaumasite structure can tolerate the replacement of only 1/8 Si by Al. On the ettringite side of the gap, the compositional range is wider; ettringite can tolerate the replacement of 1/2 its Al by Si. The immiscibility can be explained in terms of changes in anion site occupancy and ordering in the channels of the structure.

Two morphological types were observed by TEM and seemed to be correlated with the two structure types identified by XRD. However, EDX analysis (Fig. 7) was unable to distinguish the gap in the compositional range determined by FTIR. A high degree of variation in crystal composition was a characteristic of these analyses, suggesting nonequilibrium conditions or influences from other phases. The excess Si observed by this method appears to be associated with the amorphous secondary phase and may be associated with the tetrahedrally coordinated Si observed in the FTIR spectra.

The location of this miscibility gap explains the compositional range of thaumasite observed in concrete affected by TSA. In these cases, the thaumasite phase formed has a composition close to $Ca_3Si(OH)_6SO_4CO_3{\cdot}12H_2O$. On the thaumasite side of the miscibility gap, only a narrow range of compositions is possible. The location and extent of immiscibility prevent thaumasite with higher levels of aluminium in its structure from forming in concretes.

The formation of thaumasite–ettringite solid solutions is significant in investigation of the TSA for several reasons. Firstly, the similarity between the thaumasite and ettringite structures, and hence the XRD patterns of these and intermediate compositions, leads to problems in identification by XRD. While the thaumasite and ettringite end members can be distinguished by careful measurement of peak positions, the presence of solid solutions would make it very difficult to identify the nature of the thaumasite/ettringite phase formed by measurement of d-spacings alone.

Secondly, the presence of reactive alumina, usually in the form of ettringite, is known to assist in thaumasite formation. The formation of solid solutions has previously been observed as a precursor to thaumasite formation [8,29,30]. It would appear likely, therefore, that the solid solution between thaumasite and ettringite could play a role in initiating thaumasite formation.

This work has determined the miscibility gap between ettringite and thaumasite. Research is continuing to assess the stability of these solid solutions, and to determine the role of alumina in initiating or accelerating thaumasite formation.

Acknowledgments

We would like to thank the Engineering and Physical Sciences Research Council, UK, for financial support of this work (grant number GR/M37714/01). We would also like to thank Dr. Iain Marr (Department of Chemistry, University of Aberdeen) for useful suggestions.

References

[1] H.F.W. Taylor, Cement Chemistry, 2nd ed., Thomas Telford Publishing, London, 1997.
[2] Report of the Thaumasite Expert Group, The thaumasite form of sulfate attack: Risks, diagnosis, remedial works and guidance on new construction, Her Majesty's Stationery Office, London, 1999.
[3] Department of the Environment, Transport and the Regions, Thaumasite Expert Group one-year review, http://www.construction.detr.gov.uk/thaumasite/oneyear/index.htm.
[4] N.J. Crammond, Thaumasite in failed cement mortars and renders from exposed brickwork, Cem. Concr. Res. 15 (1985) 1039–1050.
[5] J. Bensted, Thaumasite — background and nature in deterioration of cements, mortars and concretes, Cem. Concr. Compos. 21 (2) (1999) 117–121.
[6] R. Lachaud, Thaumasite et ettringite dans les matériaux de construction, Ann. Inst. Tech. Batim. Trav. Publics 32 (1979) 370–373.
[7] H. Kollmann, G. Strübel, Ettringite–thaumasite mixed crystals of Brenk (Eifel), Chem. Erde 40 (1981) 110–120.
[8] H. Kollmann, G. Strübel, F. Trost, Mineral synthetic tests to find the causes of expansion through Ca–Al–sulfate hydrate and Ca–Si–carbonate–sulfate hydrate, Tonind.-Ztg. 101 (3) (1977) 63–70.
[9] S.A. Stronach, Thermodynamic modelling and phase relations of cementitious systems, PhD Thesis, University of Aberdeen, 1996.
[10] S.J. Barnett, C.D. Adam, A.R.W. Jackson, Solid solutions between ettringite and thaumasite, J. Mater. Sci. 35 (16) (2000) 4109–4114.
[11] R.A. Edge, H.F.W. Taylor, Crystal structure of thaumasite, Acta Crystallogr., Sect. B 27 (1971) 594–601.
[12] A.E. Moore, H.F.W. Taylor, Crystal structure of ettringite, Acta Crystallogr., Sect. B 26 (1970) 386–393.
[13] H. Effenberger, G. Will, E. Zobetz, A further refinement of the crystal structure of thaumasite, $Ca_3Si(OH)_6SO_4CO_3 \cdot 12H_2O$, Neues Jahrb. Mineral., Monatsh. 2 (1983) 60–68.
[14] J. Zemann, E. Zobetz, Do the carbonate groups in thaumasite have anomalously large deviations from coplanarity? Sov. Phys. Crystallogr. 26 (6) (1981) 689–690.
[15] R. Berliner, in: M.D. Cohen, S. Mindess, J. Skalny (Eds.), Materials Science of Concrete — The Sydney Diamond Symposium, American Ceramic Society, Westerville, Ohio, 1998.
[16] L.J. Struble, Synthesis and characterisation of ettringite and related phases, Proceedings of the VIIIth International Congress on the Chemistry of Cement, 1987, pp. 582–588.
[17] S.J. Barnett, D.E. Macphee, in preparation.
[18] http://www.ccp14.ac.uk/ccp/web-mirrors/commercial/siroquant/siroqnt/online.htm
[19] J.I. Langford, D. Loüer, Powder diffraction, Rep. Prog. Phys. 59 (1996) 131–234.
[20] E.P. Flint, L.S. Wells, Analogy of hydrated calcium silicoaluminates and hexacalcium aluminate to hydrated calcium sulfoaluminates, J. Res. Natl. Bur. Stand. 33 (1944) 471–478.
[21] S.P. Varma, J. Bensted, Studies of thaumasite, Part I, Silic. Ind. 38 (1973) 29–32.
[22] J. Bensted, S.P. Varma, Studies of thaumasite, Part II, Silic. Ind. 39 (1974) 11–19.
[23] R.B. Perkins, C.D. Palmer, Solubility of $Ca_6[Al(OH)_6]_2(CrO_4)_3 \cdot 26H_2O$, the chromate analogue of ettringite; 5–75 °C, Appl. Geochem. 15 (2000) 1203–1218.
[24] R.B. Perkins, C.D. Palmer, Solubility of ettringite ($Ca_6[Al(OH)_6]_2(SO_4)_3 \cdot 26H_2O$) at 5–75 °C, Geochim. Cosmochim. Acta 63 (1999) 1969–1980.
[25] T.L. Hughes, C.M. Methven, T.G.J. Jones, S.E. Pelham, P. Fletcher, C. Hall, Determining cement composition by Fourier transform infrared spectroscopy, Adv. Cem. Based Mater. 2 (1995) 91–104.
[26] V.C. Farmer (Ed.), The Infra-Red Spectra of Minerals, Mineralogical Society, London, 1974.
[27] H. Pöllmann, H.-J. Kuzel, R. Wenda, Solid solution of ettringites: Part I. Incorporation of OH^- and CO_3^{2-} in $3CaO \cdot Al_2O_3 \cdot 3CaSO_4 \cdot 32H_2O$, Cem. Concr. Res. 20 (1990) 941–947.
[28] S.J. Barnett, C.D. Adam, A.R.W. Jackson, An XRPD profile fitting investigation of the solid solution between ettringite, $Ca_6Al_2(SO_4)_3(OH)_{12} \cdot 26H_2O$, and carbonate ettringite, $Ca_6Al_2(CO_3)_3(OH)_{12} \cdot 26H_2O$, Cem. Concr. Res. 31 (2001) 13–17.
[29] M.A. Halliwell, N.J. Crammond, Two-year report on avoiding the thaumasite form of sulfate attack, BRE Lab Report, BR385, CRC, UK, 2000.
[30] S.J. Barnett, M.A. Halliwell, N.J. Crammond, C.D. Adam, A.R.W. Jackson, Study of thaumasite and ettringite phases formed in sulfate/blast furnace slag slurries using XRD full pattern fitting, submitted.